Oxidation catalysis on Pt and Au : complexity of simple chemistry

Spronsen, M.A. van

Chapter 2

Oxidation of Pt(111) at high pressure and temperature; formation of surface oxides

2.1 Introduction

Platinum serves as one of the components in the automotive catalyst. In this car catalyst, CO and residual hydrocarbons are oxidized to CO_2. In addition, NO is reacting with O_2 to form NO_2 when the car catalyst is operating in lean burn, i.e., in excess oxygen.

To improve catalysts by rational design, it is crucial to fully understand the interaction of oxygen with a realistic Pt catalyst as used in the catalytic car converter. A first step towards this goal is to gain understanding on the O_2 interaction with a well-defined model catalyst. In its most essential form, this is the extended Pt(111) surface. This surface is the lowest in surface energy and expected to be the dominant facet of (larger) particles [29].

The adsorption and dissociation of O_2 on Pt(111) have been extensively studied under traditional surface science conditions, i.e., UHV. It was found that O_2 binds molecularly below 160 K with a saturation coverage of $\frac{4}{9}$ monolayer (ML) [30, 31]. At higher temperatures, O_2 dissociates readily to form a p(2×2)-O chemisorbed overlayer with a saturation coverage of 0.25 ML. Oxygen structures with higher coverage could be obtained by O_2 exposure at elevated temperatures [32]. Using NO_2 the saturation coverage was doubled and a p(2×1) structure was observed by STM [33].

Stronger oxidants, such as O_3 [34] and atomic oxygen [35, 36], were needed to create Pt oxides, These oxides resulted in O coverages above approximately 1 ML and were accompanied by chemical shifts in XPS and so-called explosive desorption in temperature-programmed desorption (TPD). An interesting surface oxide was discovered after oxidizing the Pt(111) surface with NO_2 [33]. This surface oxide has a structure distinctly different from α-PtO_2. The surface oxide's structure was a one-dimensional (1D) chain of 7 Pt atoms each surrounded by four O atoms and expanded along the direction of the chain, to acquire a separation comparable to the lattice of α-PtO_2. These chains were interpreted as having a chemical composition of PtO_2. To derive this composition, only the Pt atoms in the chain were considered as being oxidized. The chains assembled in a 'honeycomb'-superstructure, between which O resided.

Surface science studies performed under vacuum conditions do not guarantee to identify the surface structure under realistic reaction conditions for catalytic oxidation. The relevant structure can only be elucidated when the structure is probed in situ, i.e., at high pressure and elevated temperatures. Two independent in situ SXRD studies showed the formation of bulk-like α-PtO_2 [37, 38]. Both studies do not report the formation of any surface oxide. These observations seem to contradict with a near-ambient-pressure XPS study [39], which showed the formation of a surface oxide at similar temperatures as in the SXRD experiments, but at much lower pressures. This surface oxide was found to be an intermediate in the bulk oxidation of Pt.

The most important questions remain unanswered. What is the structure of Pt in a oxidation catalyst under catalytically relevant conditions, i.e., at high temperature and high O_2 partial pressure? Is this a surface oxide or a bulk oxide? If it is a surface oxide, is its structure identical to the UHV-formed surface oxide?

Using the ReactorSTM [19], we studied the oxidation of Pt(111) with O_2 pressures of 1–5 bar in a temperature range of 300–538 K. We observed the formation of two

stable surface oxides. The first had a spoked-wheel structure, in which equilateral triangles were arranged into spoked wheels. The lattice constant within the spokes was expanded similarly to the building blocks of the surface oxide formed after NO_2 exposure of Pt(111) in UHV [33]. The spoked-wheel structure can be regarded as an oxygen-rich version of the previously reported surface oxide, which lacked the spokes and showed only a hollow honeycomb. The second discovered structure consisted of a pattern of rows with a periodicity of $\sqrt{3}$a. These rows were lifted from the surface and consisted of half the Pt atoms in the top layer. The structure's unit cell was $(2\times n)$ with $n=8$ if we would assume similarly expanded rows as building block. Based on the expanded rows which agreed well with the α-PtO_2 lattice constant, we conclude that both structures were surface oxides and not mere chemisorption structures. For these surface oxides, it is not trivial to determine the chemical composition, because it is not clear if only the Pt atoms in chains were oxidized. If this would be assumed, than the Pt oxide would best be described as PtO_2 chains. Interestingly, the formation of α-PtO_2 was not observed. The conclusions from the experiments described in this chapter will be given at the end of Chapter 3, together with the conclusions derived from the experiments presented in that chapter.

2.2 Experimental

All experiments were performed in a ReactorSTM. This system has recently been described in great detail [19]. Therefore, only its most important aspects are repeated here. The ReactorSTM is a UHV system housing a small-volume (0.5 ml) flow-cell reactor. This reactor is integrated with a home-built miniature STM. The design is such that all delicate STM parts are outside the reactor and not exposed to gases or to elevated temperatures. Only one surface of the sample and the tip with its sliding tip holder are inside the reactor. To seal the high-pressure reactor from the UHV chamber, a fluoroelastomer seal[1] is used. In this way, we maintain UHV conditions in the surrounding chamber, even when the reactor pressure reaches 6 bar. The fluoroelastomer limits the temperature of the high-pressure experiment to 600 K. The temperature is measured with a K-type thermocouple, laser spot welded to the side of the sample. In both the sample holder and transfer system, the thermocouple connections include some non-thermocouple material. An extensive calibration was performed with a second true K-type thermocouple. This resulted in an error of all temperatures of less than 1 %. Details of this calibration are included in the supplementary information (SI). The sample is heated with a filament placed on the vacuum side of the sample. In addition, the system houses equipment to study the sample with low-energy electron diffraction (LEED), Auger electron spectroscopy (AES), and XPS, which we can employ before and after high-pressure exposure of the sample.

The platinum single crystal was polished to the (111) plane within 0.1°, confirmed with Laue diffraction[2]. After polishing, it was cleaned in the UHV system by Ar^+

[1] ^{TM}Kalrez® 7075 [40]

[2] Surface Preparation Laboratory [41], Czochralski-grown, purity of 5N

sputtering[3,4] and annealing both in O_2[3,5] and in UHV[6]. At least 60 to 70 of these cycles were performed before starting the first experiment and around 5 cycles were completed between consecutive experiments. The preparation method was routinely checked with both LEED[7] and AES[8]. The LEED pattern showed sharp spots with a (1×1) periodicity (SI, Fig 3.8), at energies down to 35 eV. In addition, AES showed that the surface was free of contaminants, such as O or C.

Gases were handled with a dedicated gas handling system, previously described in detail [19, 42]. This system allows exposing the surface to a mixture of up to 5 different gases in a wide range of partial pressure ratios and flows. The gases[3] were used without further purification. Unless specified otherwise, all experiments were performed at a total normal flow, i.e., the flow at a pressure of 1 bar, of 10 ml/min with 83.3 % O_2 and 16.7 % Ar.

STM tips were prepared by mechanically cutting a PtIr wire[9]. These tips were used without further in situ treatments. STM measurements were performed in constant-current mode using a video-rate STM controller [42, 43]. All images were recorded from top to bottom with the fast scan direction from left to right. Both planar and linear line-by-line background subtractions were employed. In order to emphasize local height variations, several images are presented in differentiated form with the color indicating the local slope measured from left to right. No nonlinear filtering was applied unless stated otherwise. To calibrate the piezoelectric scan element, atomically resolved Au(111)[10] STM images were used. These images were recorded with a closed reactor, with a seal in place at room temperature. This resulted in a calibration with a standard deviation of 1.5 %. Additional inaccuracy could stem from changes in the behavior of the scanner at reaction conditions compared to UHV. However, test observations of Au(111) under reaction conditions suggest that this effect is small.

2.3 Results

2.3.1 Exposure to 1.0 bar O_2 at 530–540 K

Network of islands

Figure 2.1a shows an STM image of the freshly prepared Pt(111) surface, in the reactor with the seal in place, at room temperature, prior to high-temperature O_2 exposure. It demonstrates that we started with a flat surface with wide terraces of typically between 10 nm and 120 nm. In addition, the steps were generally straight with only very few pinning sites. In the STM image, some slightly brighter spots

[3] O_2: Praxair 5.0N and CK 4.5N and Ar: Linde 6.0N, Westfalen 5.0N, and Praxair 5.0N
[4] ∼20 minutes, beam energy of 1.0 keV, and sample current of 3–4 μA
[5] ∼2 minutes at 948 K in 1×10^{-7} mbar O_2
[6] at 1130 K for ∼10 minutes; last cycle at 1129 K
[7] Omicron SPECTALEED, 4 grid
[8] Omicron SPECTALEED, retarding-field analyser
[9] Goodfellow, Pt/Ir ratios of 90/10 or 80/20, ⌀ = 0.25 mm
[10] Surface Preparation Laboratory [41], polishing accuracy of ∼0.1°, Czochralski-grown, purity of 5N

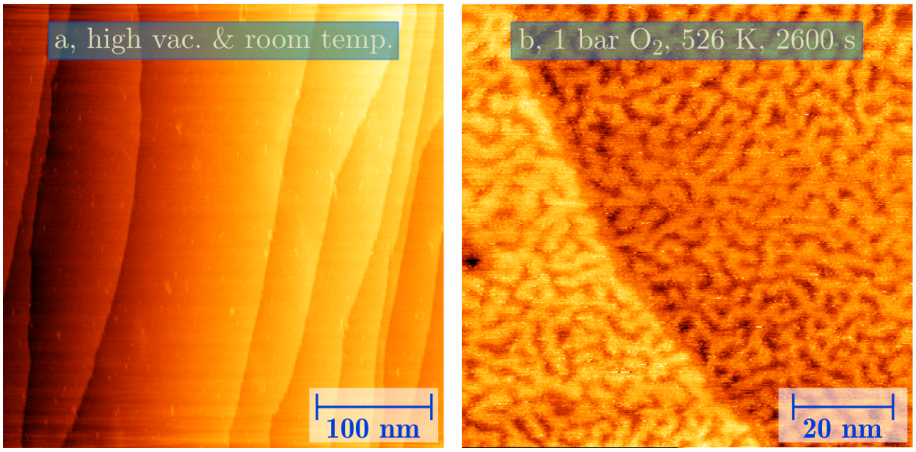

Figure 2.1: Two STM images showing the change in large-scale morphology upon high-pressure O_2 exposure. (a), freshly prepared Pt(111) surface in the reactor in high vacuum at room temperature (382×386 nm^2, $U_{bias} = 0.25$ V, $\overline{I_{tunnel}} = -0.07$ nA, $t_{image} = 71$ s). (b), stable, oxidized surface at 1.0 bar O_2 and 531 K after 43 minutes exposure (94×92 nm^2, $U_{bias} = 0.04$ V, $\overline{I_{tunnel}} = -1.08$ nA, $t_{image} = 35$ s). Nonlinear filtering was applied to remove artefacts due to vibrational interference of the microscope.

were visible. The nature of these spots was unknown but we assumed that they originated from the residual gas that the surface was exposed to in the reactor, prior to high-pressure gas exposure. In this initial part of the experiment, the reactor volume was connected to the vacuum of the surrounding UHV chamber via a set of narrow pumping lines. In general, the spots disappeared when the O_2 flow was started.

Upon admission of the high-pressure O_2 atmosphere, the surface immediately started to change. This phase was very dynamic and contained rapidly changing structures. These will be discussed later, after we focus on the stable structure. This dynamical phase lasted around 30–50 minutes, after which the surface adopted a large-scale stable configuration. A typical example of this configuration is visualized in Figure 2.1b. This in situ STM image exhibits a monoatomic step from the top left corner to the middle of the bottom edge. The step height equaled 0.22 ± 0.04 nm as measured on four separate height profiles. Although the error bar was large, it agreed very well with a monoatomic step of Pt(111) of 0.23 nm. Hence, the imaged surface consisted of two levels of terraces. Within each terrace, the surface showed a complicated network of worm-shaped islands.

The islands divided each terrace in two levels. Figure 2.1b suggests that the top level of the lower terrace was at the same height as the lower level of the upper terrace. In other words, the image seems to indicate that the island structure divided each terrace over two height levels of the Pt(111) surface.

To further substantiate this notion, we quantified the depth of the valleys in between the islands. The measured depths were most reliable for the widest valleys. This

was because the macroscopic tip could not penetrate the narrowest valleys if their width was smaller than the tip apex. The depth was analyzed for several line profiles and a value of 0.21±0.02 nm was obtained and agreed well with a monoatomic step. Therefore, we conclude that solid, flat terraces transformed into networks of monoatomic-high, worm-shaped islands upon O_2 exposure. Through the valleys, the lower lying terrace became visible. This resulted in a two-level terrace structure.

Spoked-wheels structure

Parallel to the formation of the large-scale structure, both the islands and the valleys in between developed an extended pattern of triangles. These structures were not observed directly after the onset of the exposure. The first triangles were observed after a time period of 17–33 minutes, which was on the same time scale as needed to form the stable worm-shaped island network discussed in the previous section. During this period, the dynamics of the surface was too prominent to obtain atomic resolution.

The triangles formed a close-packed network resulting in a 'spoked-wheel' superstructure. This structure is presented in Figure 2.2. In the left panels of this figure, the background-subtracted height images are given. In addition, the right panels show differentiated versions of the same images, in order to highlight the atomic contrast more strongly.

These images show that the spoked-wheel structure extended over tens of nanometers covering multiple islands. Figures 2.2a and 2.2a' show the spoked-wheel structures in one island. The island slowly moved to the bottom left due to thermal drift. In Figures 2.2b and 2.2b', a second island is visible. The third STM image (Figures 2.2c and 2.2c') shows the atomic resolution on the second island. More interestingly, it shows that the spoked-wheel structure continued in the valleys between these islands. This can be clearly seen when the differentiated STM image is compared to the linearly corrected STM image. The former shows a continuing network of spoked wheels in a large region of the surface. The latter, nondifferentiated STM image, clearly showed that this network spanned (part of) two islands and the void in between.

An intrinsic determination of the in-plane drift velocity was established by studying the triangle angles. These angles should all be 60° for equilateral triangles. The assumption that the observed structure formed equilateral triangles was justified by the three-fold nature of the surface and the fact that different rotational domains were not observed. After drift correction, the length of the spokes was found to be 2.2±0.1 nm. This length corresponded to 7.9±0.4 Pt(111) lattice constants.

Interestingly, the highest atomic contrast was obtained for very small bias voltages of ∼50 mV. Several images, such as Figures 2.2c' and 2.3c show clear atomic resolution within the rows. The interatomic distance in the spokes was quantified by exclusively analyzing the spokes parallel to the fast scan direction. Measurements in this direction should hardly be affected by in-plane drift [44]. Consequently, they should also hardly depend on the quality of drift correction. The measured atomic periodicity in the rows was 0.30±0.01 nm, which was significantly larger than the Pt(111) lattice constant of 0.28 nm. The measured value was very close to the lattice constant found for the previously reported surface oxide, which was 0.31 nm. Also, it was close to the

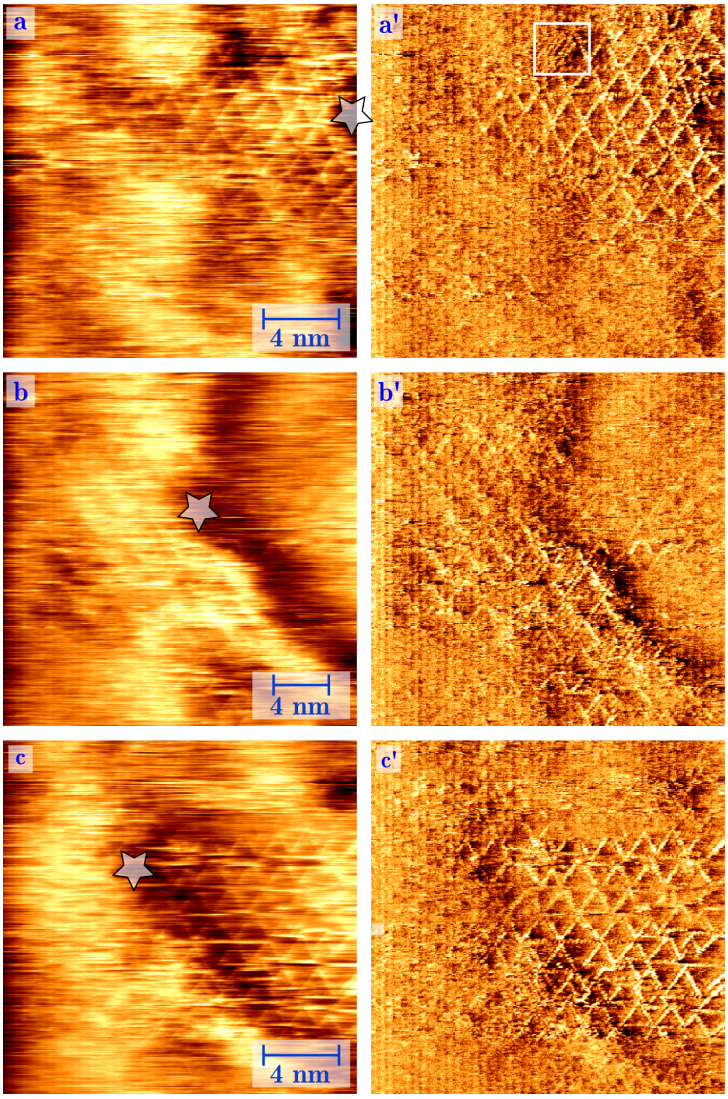

Figure 2.2: STM images (25×25 nm^2, U_{bias} = 0.05 V, I_{tunnel} = –(0.86–0.87) nA, t_{image} = 8.4 s) illustrating the formed spoked-wheel structure on the islands and valleys on a single terrace upon exposure to 1.0 bar O_2 at 529 K. Field of view was gradually moving to the right of the images due to thermal drift. The white star provides a marker of reference. The STM images are shown with linear background subtraction (a, b, and c) and with a line-by-line differentiated background correction (a', b', and c'). The latter enhances the contrast of the spoked wheels. The exposure times to O_2 were around 32–33 minutes. The white rectangle in (a)' shows a small patch of remaining, transient, distorted-hexagonal structure.

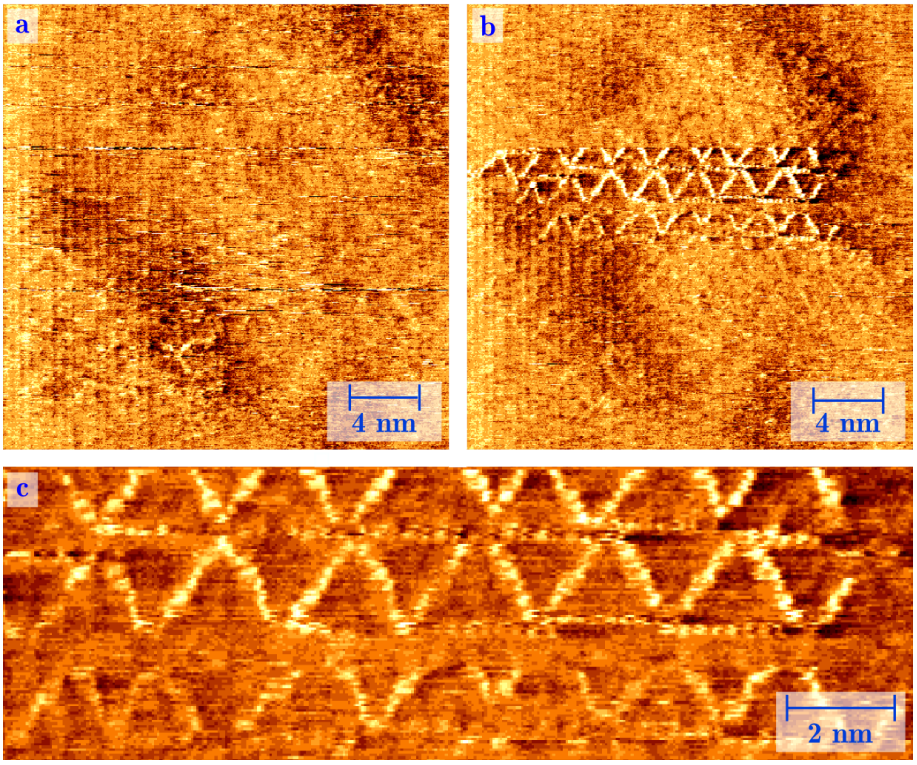

Figure 2.3: STM images (line-by-line differentiated) showing the detailed atomic resolution of the spoked-wheel structure. (a), STM image with typical resolution of the surface exposed to 1.0 bar O_2 at 529 K for 33 minutes (25×25 nm^2, $U_{bias} = 0.05$ V, $\overline{I_{tunnel}} = -0.87$ nA, $t_{image} = 8.4$ s). (b), subsequent STM image, in which a switch in the tip state resulted in significantly improved resolution, STM settings as in (a). (c), enlargement of the central region in (b) with adjusted color scale to enhance the atomic contrast.

α-PtO_2 [45–49] and PtO [45, 49, 50] lattice constants of 0.31 ± 0.00 nm.

The atomically resolved STM images revealed that most spokes consisted of 8 atoms including both endpoints, with very few being extended to 9 or more atoms. This suggested that there was a clear preference for this structure to form spokes with a length of 8 atoms, including both endpoints, corresponding to 7 interatomic distances. Given the spoke length of these spokes of 2.2 ± 0.1 nm, this would lead to a periodicity within the row of 0.31 ± 0.01 nm. The measured periodicity matches very well to the previously observed surface oxide [33] and to the bulk oxides, α-PtO_2 and PtO.

The apparent height of the spokes depended on the exact state and/or shape of the tip apex and was found to range from 0.03 nm to 0.11 nm at the same bias voltage of 0.05 V (Table 3.1, SI). Both measurements were taken with the same STM tip, but

between the experiments the tip (gently) crashed into the surface, which most likely had changed the apex of the tip either in shape or in chemical composition. In addition, when the bias voltage was changed between 0.01 V and 0.10 V (in the same experiment), a small variation was observed. In these measurements, the apparent height changed from 0.10 nm for 0.01 V to 0.12 nm for 0.10 V, but this variation was less than the standard deviation on these measurements (0.03–0.06 nm). In all cases, the measured apparent heights were much smaller than the Pt(111) monoatomic-step height.

Transient, distorted-hexagonal structure

Before a stable, extended area of spoked wheels was formed, the surface was dynamic and transient structures were observed. This stage is summarized in Figure 2.4a, which shows a high-resolution STM image of typical transient structures. In this STM image, several triangles could be noticed in a few locations and they were starting to form spoked wheels. In addition to these emerging spoked wheels, a row-like structure could be distinguished. This structure, in fact, showed a hexagonal-like symmetry in the highest resolution regions of the image (see regions close to the arrows, Figure 2.4a).

A perfect hexagonal lattice can appear as rows in one of the directions of the lattice due to a minor asymmetry in the tip apex, i.e., the STM tip is not as sharp in one of the directions as in the other two. This asymmetry results in a somewhat poorer resolution and the image appears to have rows in that direction. However, in Figure 2.4 this was definitely not the case, since the upper region of the STM image showed three rotational domains (blue, black, and green arrows, Figure 2.4a) within single scan lines. For this to be an STM tip artefact, the STM tip should have changed its apex several times per scan line at more or less the same positions. This seems highly unlikely since the STM conditions were such that very stable STM feedback was obtained in this part of the experiment.

There is a second explanation for the observation of these rows, which requires anisotropy in the observed lattice, i.e., different lattice constants in different directions. If these lattice constants are in the order of the best attainable resolution of a particular STM tip, then the direction of the smallest lattice constant is not resolved completely and the structure appears as rows. This occurs even with a perfectly symmetric STM tip. This means that the observed lattice (Figure 2.4a) had, in fact, a distorted-hexagonal structure, in which the lattice was expanded perpendicular to the rows. The three rotational domains were all distinguished in Figure 2.4a (blue, black, and green arrows).

The distorted-hexagonal structure was characterized by studying the fast Fourier transform (FFT) of the region indicated by the white square in Figure 2.4a. The FFT image is represented in Figure 2.4b. It clearly shows the distorted-hexagonal pattern. The pattern was compressed along the white line indicated in Figure 2.4b. This compression in reciprocal space is equivalent with an extension in real space. The other rotational domains showed similar but rotated patterns. Therefore, the distortion could not be explained by thermal drift, because that would have affected all regions equally as they were imaged in the same time interval.

Figure 2.4a shows atomic resolution both perpendicular and parallel to the rows.

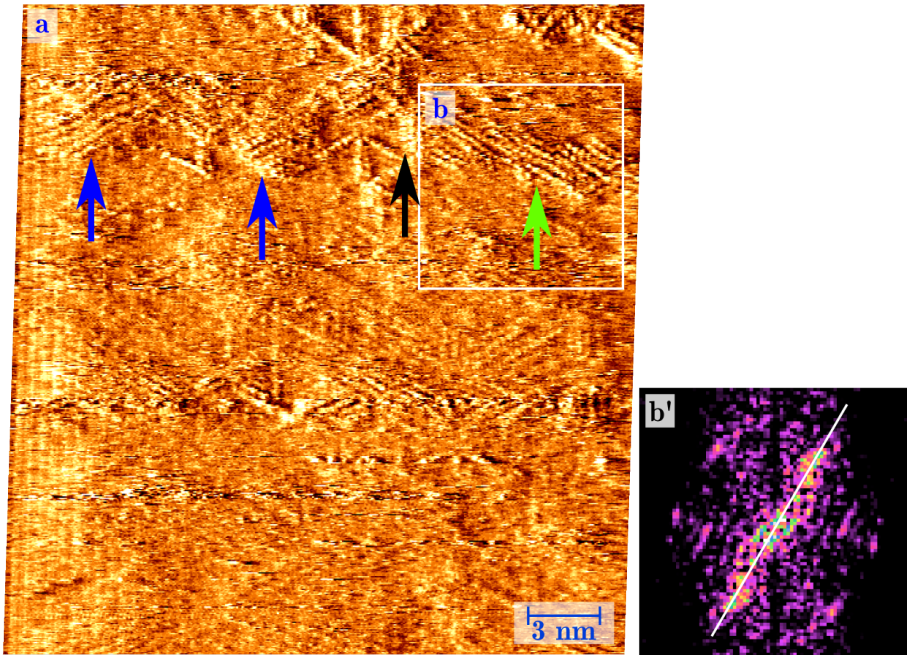

Figure 2.4: STM image (a) showing the transient structures observed before a stable spoked-wheel structure had developed on a large scale (25×26 nm^2, $U_{bias} = 0.05$ V, $\overline{I_{tunnel}} = -1.01$ nA, $t_{image} = 8.4$ s, line-by-line differentiated). Surface was exposed to 1.0 bar O_2 at 527 K for 18 minutes. Colored arrows indicate different rotational domains of the distorted-hexagonal structure. (b), fast Fourier transform (FFT) calculated from the region in the white square of (a). The white line indicates the axis of reciprocal-space compression of the hexagonal structure.

The lattice constant within the rows was determined by measuring the corresponding spots in the FFT image (Figure 2.4b). A lattice constant of 0.30±0.01 nm was found, which corresponded well to the in-spoke lattice parameter of the spoked-wheel structure, the previously observed surface oxide [33], and the lattice constant of α-PtO_2 [45–49] and PtO [45, 49, 50]. The average distance between the rows was determined directly from height profiles across several rotational domains. A value of 0.37±0.04 nm was found, which was midway between 0.24 nm and 0.48 nm ($\frac{1}{2}\sqrt{3}$ and $\sqrt{3}$ times the Pt(111) lattice constant). So, the distorted-hexagonal structure was nonepitaxial with respect to the Pt(111) lattice, perpendicular to the rows.

Minute patches of this structure remained present in the stable spoked-wheel structure. This can be seen in the region indicated by the white rectangle in Figure 2.2a'. The STM image quality was not good enough to resolve the atomic structure within the rows, but the distances between the rows matched that of the distorted-hexagonal structure.

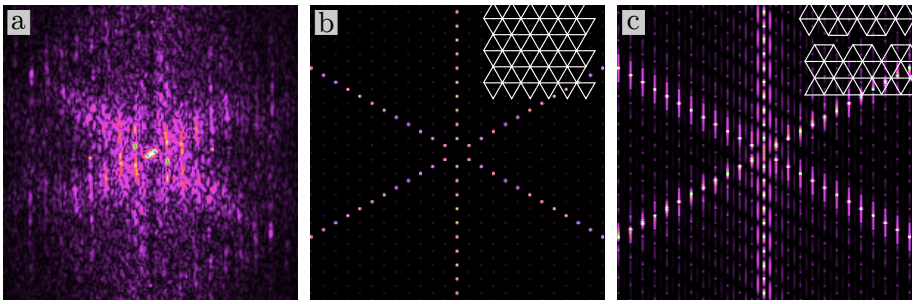

Figure 2.5: FFT of (a) STM image showing the spoked-wheel structure (Figure 2.3b), (b) perfect and extended spoked-wheel structure, and (c) spoked-wheel structure with a translational defect creating a horizontal defect line. Insets of (b) and (c) show the structures from which the FFTs were calculated.

Defects

Under the high-pressure O_2 conditions, the spoked-wheel oxide formed large domains all across the surface. However, the formed structures were not perfect and contained many defects. Some of these defects occurred only during growth, while others persisted in the stable structures. These defects can be seen in Figures 2.2 and 2.3.

The presence of these defects became clear when the FFT of Figure 2.3b was compared to the FFT calculated for a perfect spoked-wheel pattern (inset of Figure 2.5b). These FFTs are depicted in Figure 2.5a and b, respectively. The FFT of the perfect spoked-wheel structure (Figure 2.5b) was a 30° rotated spoked-wheel pattern. The spokes were comprised of individual higher order spots reflecting the distance between parallel spokes. These spots were also clearly visible in the experimentally obtained pattern (Figure 2.5a). However, the experimental spots were elongated in the vertical direction.

This vertical streakiness indicated that the structure of Figure 2.3b exhibited a translational defect that divided the pattern in two translational domains. This is visualized in Figure 2.5c in which a calculated FFT is depicted of a spoked-wheel pattern containing a horizontal translational defect. More specifically, one diagonal (top left to bottom right, Figure 2.5c) was streaked symmetrically while the other (top right to bottom left, Figure 2.5c) was asymmetrically elongated alternating in top and down direction. This asymmetric behavior was also visible in the experimental FFT. Evidence of these translational defects was also frequently observed in STM, which can be clearly seen in the detailed STM image depicted in Figure 2.6a and the corresponding model (Figure 2.6a').

In addition to translational defects, also other structural defects were observed. Most prominently, the incorporation of several smaller triangles in the structure. This is illustrated by Figure 2.6b. This figure shows that smaller triangles clustered. These clusters need to occupy the same space as an integer number of regular triangle(s) in order for the structure to remain close packed without voids. The smaller triangles had a minimal edge length of 1.3 nm or 4–5 Pt(111)-lattice constants.

A third class of defects was the doubling or tripling of spokes. Similar defects were

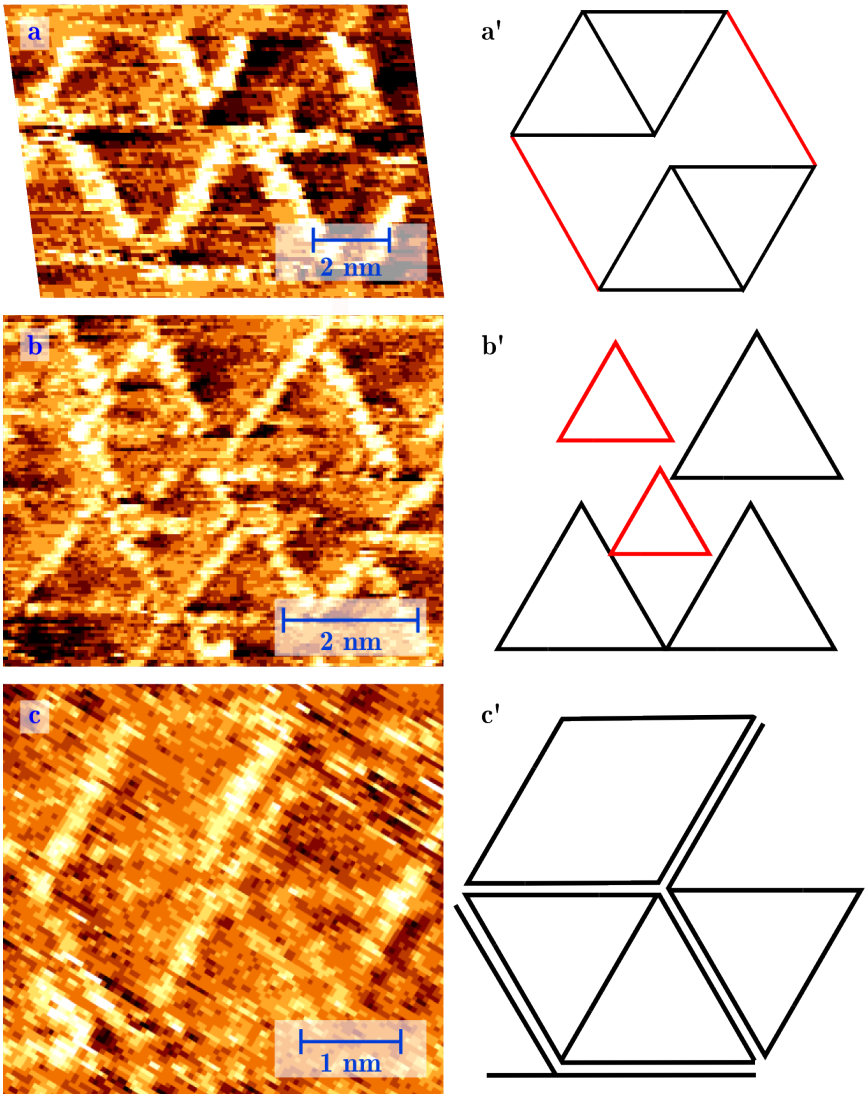

Figure 2.6: STM images with models showing various structural defects (depicted by red lines), such as translational defects (a and a'), incorporation of smaller triangles (b and b'), and doubling and missing of spokes (c and c'). All STM images were obtained at $p_{O_2} = 1$ bar and $T = 529$ K, $U_{bias} = 0.05$ V, $I_{tunnel} = -(0.89–0.98)$ nA, and the exposure times were 31, 33, and 18 minutes, respectively. The STM images are shown after line-by-line differentiation. (c) was rotated by 31° to correct for a different scan orientation and to match other STM images.

reported by Devarajan et al. [33] and Weaver [51] for the previously reported surface oxides. However, confirming the existence of multiple spokes is rather difficult by STM. The images can be heavily distorted when the tip does not end in a single apex. In this case, the STM image appears as an overlap of multiple translated images and double or triple spokes could be the result. Generally, double spokes were not frequently occurring in stable structures. In the early stages of growth, this defect was commonly observed. One example is presented in Figure 2.6c. In this case, an STM tip artefact could be excluded. This was because doubling of spokes was observed in all three directions, but not all spokes were doubled, which would be expected when a multiple tip was used for the imaging. This image also illustrates that doubling of spokes usually concurred with missing spokes.

The separation between the spokes in Figure 2.6c was equal to 0.38±0.03 nm. The error bar was rather high but not related to the thermal drift, which was estimated by following large-scale morphology movement and was, at its maximum, 1 % of the image dimensions. The calculated separation was almost equal to the row-to-row distance of the transient, distorted-hexagonal structure discussed in the previous subsection.

2.3.2 Increasing O_2 pressure

After a stable spoked-wheel structure was formed at a pressure of 1.0 bar and at 530–540 K, the O_2 chemical potential was increased by stepwise raising the O_2 partial pressure up to 5.0 bar. Starting at an O_2 pressure of 2.22 bar, a new structure was observed. An STM image showing this structure is shown in Figure 2.7. The image shows a pattern of parallel rows. This structure, that we will refer to as a lifted-row structure (see Section 2.4.1), was different from the transient, distorted-hexagonal structure discussed in section 2.3.1. It differed in two important ways, namely, it was a stable structure and the average distance between the lifted rows was much larger than the rows of the distorted, hexagonal structure (vide infra).

It is very important to note that at all the experimentally probed O_2 pressures, the spoked-wheel structure was still observed. The domains of both the spoked-wheel and lifted-row structures were rather large and estimated to be above hundred nanometer. A region several times larger than this should be analyzed to determine a statically relevant surface coverage ratio of the two structures. The large domains together with the local character of STM made determination of this ratio experimentally infeasible. Further complicating was the fact that this ratio could have been time dependent. Therefore, we cannot state anything about the surface coverage ratio of these structures nor its evolution over time.

Considering the symmetry of the lifted-row structure and that of the (111) surface, three translational domains should experimentally be observable. Different rotational domains were indeed observed in this experiment. The size of the translational domains was estimated to be in the same order as the domain size of the lifted-row structure in the mixture of lifted rows and spoked wheels. This was concluded from the absence of rotational domain boundaries.

Quantification of the thermal drift was much harder for those STM images that showed only the lifted-row structure. In these images, there was no possibility to

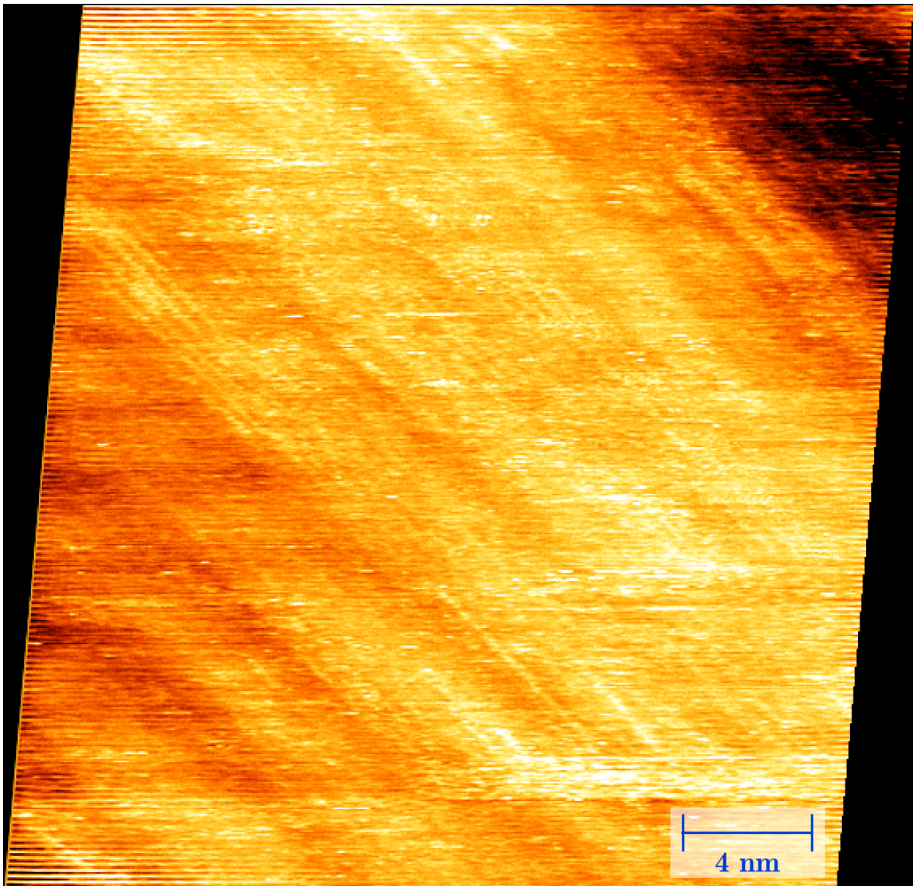

Figure 2.7: STM image in which the lifted-row structure was clearly visible, recorded at 535 K, 3.8 bar O_2, and 98 minutes in the experiment, while increasing the total pressure from 2.7 to 6.0 bar (35×27 nm^2, $U_{bias} = 0.05$ V, $\overline{I_{tunnel}} = -1.03$ nA, $t_{image} = 15.0$ s). The image is shown after drift correction and some nonlinear filtering to remove a few horizontal scan vibrations.

inherently determine the drift by the distortion of shapes with precise features, such as with the equilateral triangles of the spoked-wheel structure. In the lifted-row structure, the only atomic features consisted of parallel rows and without a priori knowledge about the row-to-row distance, drift vectors could not be determined. Instead, monoatomic steps were used to access the thermal drift velocity and a first inspection showed that thermal drift was strong in these images. A drift correction was performed based on the best overlap between consecutive images. This resulted in the elongated and sheared representation of Figure 2.7. The thermal drift was at its maximum around 30 % of the image dimensions with both the magnitude and direction changing between images.

Although the overlap was carefully optimized, it could not be guaranteed that this led to perfect drift correction, since the global morphology mainly had a one-dimensional character and because the STM images contained considerable dynamics.

After drift correction, the row-to-row distance was determined to be 0.46±0.01 nm, while it was 0.44±0.01 nm before the correction. Both these values are close to $\sqrt{3}$ times the Pt lattice constant, which equals 0.48 nm. The measured row-to-row distance is commensurate with the Pt(111) substrate and it is significantly larger than the distance between the rows of the transient, distorted-hexagonal structure (0.37±0.04 nm, Section 2.3.1).

Within the rows, the STM image of Figure 2.7 revealed weak atomic features. However, these were not ordered enough to determine a reliable lattice constant. Therefore, we derived at a (hexagonal) unit cell of (2×n)[11]. If we would assume that the rows have a similar lattice constant as the spokes of the spoked-wheel structure, n would be equal to 8. The measured height corrugation across these rows was very modest with an average value of 0.03±0.01 nm, which was in the order of a tenth of a monoatomic Pt step. Interpretation of this value requires caution as both the shape of the tip and electronic states of the tip and sample could strongly influence the measured heights.

Two translational domains should be observable, which are translated by $\frac{1}{2}\sqrt{3}$ times the Pt(111) lattice constant. In other words, either the odd or the even row in a (2×8) unit cell can be lifted. These domains were both observed and they are indicated by the cyan and light green lines in Figure 2.8a', which is an annotated replica of Figure 2.8a. The dashed lines in Figure 2.8a' correspond to rows that were missing. In two cases, those missing lines were defects within a translational domain, while the third one was a boundary between two translational domains. Because the row was missing, this boundary was identified as a light domain wall. In addition, two point defects were observed, in which a single row switched domain.

2.4 Discussion

2.4.1 Observed surface oxides

Spoked-wheel oxide

The structure observed between 1 and 5 bar O_2 consisted of closed-packed triangles, which led to the formation of a spoked-wheel superstructure. The building blocks of these triangles, i.e., the edges or spokes, consisted of Pt atoms that were expanded with respect to the metallic Pt lattice constant (0.30 ± 0.1 nm vs. 0.28 nm). This expanded lattice constant matched very well to the experimentally determined lattice constants of α-PtO_2 [45–49] and PtO [45, 49, 50] of 0.31 ± 0.00 nm. This was supported by density functional theory (DFT), calculating values of 0.32±0.00 nm [52–56] and 0.31±0.00 nm [54, 55, 57], respectively. Furthermore, β-PtO_2 contains Pt atoms with similar separation [58]. Based on this agreement, we believe that the best way to describe this structure is as a surface oxide comprised of 1D oxide rows. This

[11] $\sqrt{3}/\sin(60°)=2$

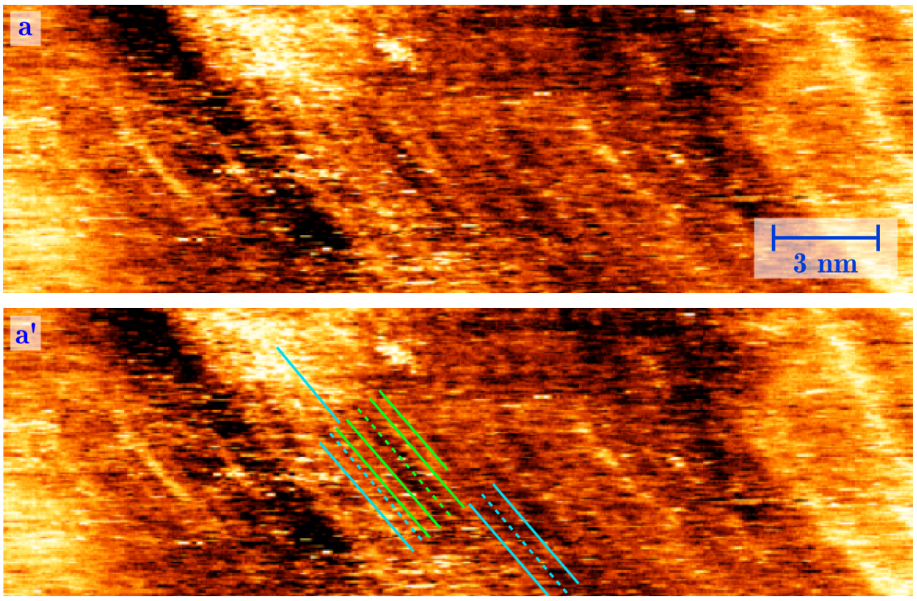

Figure 2.8: Two replicas of a zoom-in of an STM image of the Pt(111) surface exposed to 3.7 bar O_2 at 535 K and 98 minutes in the experiment, while increasing the total pressure from 2.7 to 6.0 bar. In this region, the lifted-row structure covered the surface. The lines indicated in (b) showed several interesting features, missing rows, a light domain wall, and point defects. (8×25 nm^2, $U_{bias} = 0.05$ V, $\overline{I_{tunnel}} = -1.02$ nA, $t_{image} = 4.7$ s). The image is shown without drift correction but with a modest amount of nonlinear filtering to remove a few horizontal scan vibrations.

description was supported by the XPS measurements that will be discussed in more detail in the next chapter. In short, in these experiments, the Pt(111) sample was removed from the high-pressure reactor after O_2 exposure and transported in UHV to the XPS chamber. The spectra showed a shift of the O 1s peak to 530.7 eV. This value was in the range of oxidized Pt and, more specifically, it matched very well to the surface oxides on Pt(110) [59] and Pt(531) [60]. The observed expansion suggested that Pt-Pt bonds were broken to accommodate more O atoms [33, 61]. Unfortunately, we had no direct evidence on the Pt oxidation state, so that this classification relies strongly on the comparison to related structures.

The spoked-wheel superstructure was never identified before at the low pressures of most other oxidation studies on Pt(111). It was also not predicted by theory. Nevertheless, related surface oxides were found earlier that consist of 1D oxide chains. These structures were all obtained in an artificial way, by oxidation with stronger oxidants. On Pt(111), one of these structures resembled the spoked-wheel structure and was formed by exposing the surface to a beam of atomic O [51]. Another structure was observed after exposing the Pt(111) surface to NO_2 at 450 K in vacuum [33]. The chains in this structure had a similar length (1.9–2.4 nm in Reference 33 vs.

2.2±0.1 nm in this work), but were forming "Y"-shaped structures that were assembling in honeycombs at a higher coverage. This honeycomb oxide can be thought of as a spoked-wheel superstructure without the inner spokes. On Pt(110), it was observed that the rows of the (1×2) reconstruction adopt an oxide-chain configuration with a (12×2)-22O unit cell [53, 62]. In both cases, the structures were formed from expanded Pt chains, although the structure on Pt(110) was described both as a chemisorption structure [59, 62] and as a surface oxide [53, 63].

In addition to flat surfaces, there was some experimental evidence that stepped surfaces also formed structures similar to the 1D oxide chains along along the ⟨110⟩ steps of the close-packed, {111}-facet type [64, 65]. The experiments in these papers relied heavily on DFT calculations to confirm the presence of the 1D structures. For the 1D oxides along the steps, a lattice expansion was not considered in the calculations and it is not certain that it was present.

STM images with the highest resolution (Figure 2.3) revealed that most spokes were 7 atoms in length, which resulted in a length of 2.1±0.1 nm given the expanded lattice constant. This value was close to the spoke length of 2.2±0.1 nm derived from the FFT analysis. This spoke length corresponded to 7.9±0.4 lattice constants and, as a consequence, the structure had an (8×8) unit cell with the distance between the Pt atoms in the oxide rows showing an expansion close to $\frac{8}{7}$.

Figure 2.9a shows a ball model of the spoked-wheel oxide. In this model, the spoked wheels are not formed on top of the surface layer but within, from where the 1D oxide rows are lifted. This conjecture is based on the measured height corrugation, which was well below the monoatomic Pt(111) step and is consistent with previous experiments [33] and DFT calculations [61, 66, 67].

In this model (and the following ones), the positions of the O atoms are based on an educated guess, as we had no direct observations of the O atoms in our experiments. The O atoms in the chain are forming square planar units with a single Pt atom in the middle. This geometry is based on the DFT calculations by Hawkins et al. [61]. These oxide rows have a chemical composition equal to PtO_2 and hence they were described as PtO_2 stripes, rows, or chains [61, 63, 66, 68]. Structurally, however, they share no resemblance with the hexagonal α-PtO_2. Instead, they are closely related to PtO and Pt_3O_4 with which they share the square planar PtO_4 motifs. Therefore, the 1D oxide rows should be considered as an intermediate oxidic phase [33].

The model shows a p(2×1)-O chemisorption phase inside the triangles, based on the observation of Derajavan et al. [33]. They showed that p(2×1)-O chemisorbed O filled the inner regions of the honeycombs. The O coordination of the Pt atoms in the corners of the triangles is more unclear as for this neither experimental nor theoretical evidence is available.

After having made these assumptions on the configuration of the O atoms, we derive an O coverage of 0.75 ML (see SI). This is 0.5 ML more than the (2×2)-O chemisorption structure, which is generally accepted to be the highest coverage obtainable with O_2 in UHV [30, 31, 69–71]. It is also higher than the O coverage of the honeycomb oxide of 0.60 ML (see SI). Although the honeycomb oxide resembles the spoked-wheel structure, our experiments showed that UHV oxidation with stronger oxidants is not guaranteed

to yield the same structure that is relevant at high pressure and temperature, although similar structures might be formed under the appropriate growth conditions [51].

The formation of the spoked-wheel oxide (and of the lifted-row oxide) resulted in large-scale restructuring of the surface. This roughening is illustrated in Figure 2.1b. The roughening led to a network of worm-shaped islands, dividing every terrace in two levels separated by monoatomic Pt(111) steps. We interpret this large-scale roughening as the consequence of the stress exerted by the surface oxides on the surface. This stress was relieved by forming the two-layer network.

Lifted-row oxide

At higher O_2 pressure, domains of the spoked-wheel oxide were observed coexisting with domains of the lifted-row structure. Although the atomic resolution within the rows was not good enough to measure a reliable lattice constant, we assume that the structure consisted of the same 1D oxide rows, making this a lifted-row oxide. The structure of this surface oxide was proposed previously, based on DFT calculations [61]. The same model was used to fit X-ray absorption spectroscopy (XAS) data after exposing the Pt(111) surface to a near-ambient O_2 pressure [39]. However, the effect of an expanded lattice constant was mentioned but neither evaluated in the XAS fitting nor in the DFT calculations. Two examples of the structural model that we propose with the 1D lattice expansion are depicted in Figure 2.9b. Due to the expansion within the rows, there are eight non-equivalent ways for the row to be positioned, along its own length direction. We can formally translate this into eight possible 'phases' for each row, which we will indicate by $n \times \frac{1}{8}$, with n running from 0 to 7.

The phases of neighboring rows can show order, such as the two examples in Figure 2.9b or they can be disordered. In the first, the lifted rows are 'in phase' ($\Delta n = 0$), which minimizes the O-O separation between adjacent stripes and is expected for attractive O-O interaction. The O-O separation is at its maximum for the second example, in which the phases between adjoining rows are shifted with half a period ($\Delta n = 4$). The latter example is more plausible for repulsive O-O interactions. The unit cells for these two configurations are (2×8) and $c(4\times8)$, respectively.

The experimental findings excluded the possible formation of structures, recently proposed on the basis of DFT calculations, such as the hybrid buckled/place-exchanged structure [66] and the (4×1) lifted-row structures enhanced with subsurface O [67]. These structures were found to be lower in energy than the (2×1) lifted-row structure proposed by Hawkins et al. [61]. The relative instability of the lifted-row structure in these calculations could be due to the neglect of the expansion of the Pt oxide rows. This expansion could lower both the repulsive interaction along each row and between adjacent rows.

The chemical composition of the complete top layer of the lifted-row model is equal to PtO. Although the literature on PtO is scarce and slightly controversial, PtO was found as a (meta)stable phase [45, 49, 50, 72–79] and, if crystalline, formed a tetragonal cooperite (PtS) structure [49]. Because PtO is isostructural to PdO [45, 50],

it is insightful to mention the PdO(101)-like[12] surface oxide on Pd(100) [80, 81], which bears close structural resemblance to the model in Figure 2.9b. Interestingly, it is this (101) surface that was the most dominant in sputtered, thin PtO films [73]. This makes it very plausible that also a PtO(101) layer could form on an unreconstructed Pt(100) surface under oxidizing conditions.

Of the lifted-row oxide, different rotational domains were observed, caused by breaking of the three-fold symmetry of the (111) surface. The size of the rotational domains was on the same order as the size of the lifted-row oxide domains in the mixture of the two surface oxides. In addition, two translational domains exist of this model, which are translated by $\frac{1}{2}\sqrt{3}$a in the direction perpendicular to the rows. In other words, every even or odd row can be lifted. These translational domains can result in two types of domain boundaries, a light domain wall with a missing lifted row and a heavy domain wall, in which two adjacent rows are lifted. Only the light domain wall was observed.

In the preceding discussion, we implicitly assumed that the lifted-row oxide consisted of half of the atoms in the surface layer lifted to create these rows. However, a similar structure could be formed by either removing half of the surface atom rows, which is equivalent to adding rows on top of the surface. As for the spoked-wheel oxide, we had no conclusive evidence to make a distinction between removing/adding rows versus lifting rows. Based on the significantly smaller height difference observed in STM and supported by DFT calculations [61, 66, 67], we conjecture that the observed rows were lifted, but not added on top of the surface plane. The corresponding O coverage of the lifted-row oxide is 0.88 ML (see SI), 0.13 ML more than the spoked-wheel oxide.

The lifted-row oxide was only formed at higher O_2 pressure. This observation indicated that it is only thermodynamically stable if the chemical potential of O_2 in the gas phase is high enough to populate unfavorable adsorption sites with respect to the spoked-wheel oxide. In addition, it is likely that the increase in O coverage induced even more stress on the surface. This increased stress is completely anisotropic due to the breaking of symmetry of the lifted-row oxide in the Pt(111) surface, even leading to faceting, as observed in Figure 3.2d.

In both the spoked-wheel and the lifted-row model, any subsurface oxygen was disregarded. This was simply due to the fact that our STM experiment can neither confirm nor disprove its presence. The same holds for our XPS measurements (see next chapter) . Although they seemed to suggest a single O 1s state, it is possible that there were unresolved O states. Drawing conclusions from the XPS measurements, is in particular difficult because there is no consistency in the literature with respect to the binding energy of subsurface O. Values for the binding energy are scarce and scattered: ranging from 528.5 to 531 eV [82–87] for Ag and Pd.

Oxygen penetration to subsurface sites has shown to be kinetically feasible at these temperatures [88]. Subsurface sites below the lifted Pt oxide rows could be energetically accessible [67]. This could function as an important step between the formation of surface and bulk oxides.

The O coverage estimate derived from XPS (see next chapter) was 0.88 ML. This suggested that at these conditions (1.0 bar O_2 and 441–444 K), the surface was

[12] with a $(\sqrt{5}\times\sqrt{5})$R27° unit cell

covered by a single layer of surface oxide. The estimated error bar of this value was estimated to be around 0.1 ML based on fitting results. It suggested that a mixture of spoked-wheel and lifted-row oxides was present on the surface. However, that coverage estimate (see next chapter) was a lower estimate due to the instability of the structure under vacuum conditions.

An interesting feature of Figure 2.7 can be observed when inspecting the larger scale morphology of the surface. This morphology showed an alternating pattern of higher and lower lying stripes from the top left to lower right of the image. The period of these alternating stripes was 3.7±0.4 nm, with the lower and upper-lying stripes being almost equal of width. Furthermore, the image revealed that both the higher and the lower lying stripes exhibited the same characteristic row pattern. The height difference between the two levels was determined to be 0.04±0.01 nm. Although this height difference was small, we speculate that the two stripes are small terraces at two different height levels, separated by a monoatomic step. This structure can be regarded analogous as to the two-level-islands structure discussed (vide supra) for the spoked-wheel structure. The origin of these structures could also be similar, i.e., a mechanism to reduce the stress on the surface induced by the formation of these oxygen-rich structures. The low height variation could be explained by an STM tip with a very large radius of curvature that was not able to correctly image the lower lying stripes. This tip should have one atom partially protruding, with which the lifted rows were sharply imaged. The large apex radius of the STM tip was supported by the height of the step separating the top right from the middle region of the STM image (Figure 2.7). This step was 0.15±0.02 nm, which was much smaller than the monoatomic step height of 0.23 nm even though this terrace was relatively wide, around 6 nm. Alternatively, it could be possible that stress relaxation created a pattern of alternating low and high regions with a height difference much smaller than an atomic step.

Transient, distorted-hexagonal structure

The reported transient structure showed a distorted-hexagonal lattice. In one direction, it was expanded with respect to the Pt(111) lattice, matching the lattice of α-PtO_2 very well. Perpendicular, a lattice constant of 0.37±0.04 nm was found. The Pt content of this structure was around $\frac{0.28}{0.30} \times \frac{0.28}{0.37} \approx 0.70$ compared to a Pt(111) ML. We had no information on the position and number of O atoms in this structure. If we would assume a PtO_2 composition, we would derive an O coverage of around 1.4 ML. This would be higher than the O coverage of the stable surface oxides. This higher O content of the transient structure with respect to the stable surface oxides seems counterintuitive, since it would exceed the O coverage that the surface acquired at even higher O_2 pressures. The structure could also have had a chemical composition similar to one of the other Pt oxides, such as Pt_3O_4, [48, 76, 89–91], Pt_2O [92], or Pt_5O_6 [76, 90]. In view of these uncertainties, we will not speculate further on the O content of this structure. Furthermore, it remains unclear why this structure was anisotropically expanded, but it could be related to stress relief. After initial relaxation in one direction, the resulting stress might be too low to induce similar relaxation in the other two directions.

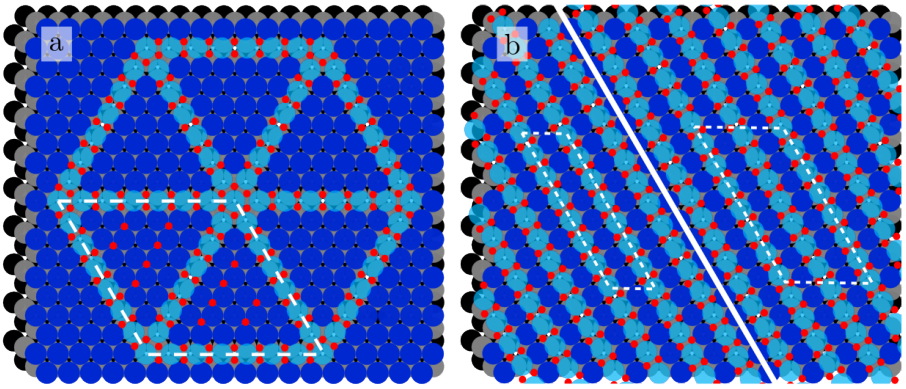

Figure 2.9: Proposed ball models of the surface oxides observed on Pt(111) with in situ STM at high pressure and temperature. Model (a) shows the spoked-wheel oxide: the spokes consist of expanded rows of Pt atoms (light blue) that are lifted with respect to the other surface atoms (dark blue). In this model, the O (red) positions were taken similarly to those proposed for other row structures [33, 61]. The spoked wheel's inner region is covered with a p(1×2)-O chemisorption structure. This structure can be described by an (8×8) unit cell, indicated by the dashed white line. Model (b) gives two examples of the lifted-row oxide in which the O atoms are ordered differently. The left side of (b) depicts the case where all lifted rows are in phase. This results in straight lines of O atoms and the smallest O-O separation, left side of (b). In the right side of (b), the largest O-O separation is obtained due to shifting of adjacent rows by half a period. These structures have a (2×8) and c(4×8) unit cell, respectively. The radii of the balls are based on the atomic radii of Pt and O.

2.5 Summary

We studied the oxidation of the Pt(111) surface in situ with STM at conditions relevant for catalysis, i.e., at an O_2 pressure of 1–5 bar and between 291–535 K. Our main findings are summarized as follows:

1. Two different surface oxides were identified. The first one was stable at all probed O_2 pressures and consisted of expanded Pt oxide stripes that assembled into triangles showing a spoked-wheel superstructure. In the proposed model, the chemical composition of this surface oxide was different from the known Pt bulk oxides. The second surface oxide was observed above 2.2 bar and showed a pattern of rows with a row-to-row distance close to $\sqrt{3}$a. We propose that it was formed from the same expanded Pt oxide rows, forming a lifted-row oxide with, most probably, a unit cell of c(4×8). The chemical composition of the top layer was PtO and structurally it resembled the PdO(101) surface oxide formed on Pd(100).
2. Parallel to the formation of these surface oxides, the surface roughened on larger length scale. This roughness was different for both surface oxides. The spoked-wheel oxide induced the formation of a two-level network of worm-shaped islands, while the lifted-row oxides produced an anisotropic surface with facets running parallel to the lifted rows.

3. Under these conditions, α-PtO_2 was not observed. The formation of the bulk oxide could be kinetically hindered under the experimental conditions, stabilizing the surface oxides. Alternatively, the surface oxides could also be thermodynamically stable phases.